Journal of Infection 91 (2025) 106609

Contents lists available at ScienceDirect

Journal of Infection

journal homepage: www.elsevier.com/locate/jinf

Viruses and Viral Diseases

Epidemiological characteristics and transmission dynamics of epidemic Japanese encephalitis in China: A modeling study

Xiaoyan Cai [a,1], Xu Wang [a,1], Haobo Ni [b,1], Jiayi Zhou [a,1], Ying Liang [c], Yunchong Yao [a], Xinyue Fang [c], Tingting Dai [a], Lingxi Wang [a], Ling Fang [d], Yi Chen [e], Yuyang Wu [e], Bo Wu [e], Wanna Zhang [e], Ruihe Zhang [e], Sen Pei [f], Xiaobo Liu [c,g,h,*], Yuantao Hao [i,**], Pi Guo [d,**]

[a] Department of Preventive Medicine, Shantou University Medical College, Shantou 515041, China
[b] National Institute of Parasitic Diseases, Chinese Center for Disease Control and Prevention (Chinese Center for Tropical Diseases Research), Shanghai, China
[c] National Key Laboratory of Intelligent Tracking and Forecasting for Infectious Diseases, National Institute for Communicable Disease Control and Prevention, Chinese Center for Disease Control and Prevention, Beijing, China
[d] Department of Pharmacy, Cancer Hospital of Shantou University Medical College, Shantou 515041, China
[e] Department of Clinical Medicine, Shantou University Medical College, Shantou 515041, China
[f] Department of Environmental Health Sciences, Mailman School of Public Health, Columbia University, New York, NY, United States of America
[g] School of Public Health, Zhejiang Chinese Medical University, Hangzhou 310053, China
[h] Xinjiang Key Laboratory of Vector-borne Infectious Diseases, Urumqi, Xinjiang 830002, China
[i] Peking University Center for Public Health and Epidemic Preparedness and Response, Department of Epidemiology and Biostatistics, School of Public Health, Peking University, Key Laboratory of Epidemiology of Major Diseases (Peking University), Ministry of Education, 38 Xueyuan Road, Beijing 100191, China

ARTICLE INFO

Article history:
Accepted 29 August 2025
Available online 2 September 2025

Keywords:
Bayesian inference
Japanese encephalitis
Mosquito-borne disease
Population movement
Transmission dynamics

SUMMARY

Objectives: In recent decades, China has experienced successive epidemics of seasonal Japanese encephalitis (JE), with the Japanese encephalitis virus (JEV) particularly spreading continuously in rural and suburban areas.

Methods: Nationwide data on 9061 JE cases, mosquito abundance from 89 surveillance sites, and population movement between 337 cities during 2013–19 were obtained. Seasonal multivariate linear regression models including time trends and reconciliation terms representing annual and semiannual cycles were fitted to the weekly time series of JE cases, and the amplitude and peak time of the cycles were estimated. A metapopulation network model of inter-city population mobility coupled with an iterative Bayesian inference algorithm was established to simulate the epidemic dynamics of JEV and estimate the time-varying transmission parameters.

Results: The timing of the annual peak of JEV epidemics varied with latitude (p-value < 0.05), mainly characterized by earlier in southern cities and later in northern cities. There was no significant difference in the annual amplitude fluctuations of JEV epidemics in different latitudes (p-value > 0.05). Regions with higher values of effective reproduction number R_{eff} were mainly concentrated in central China, including Sichuan, Chongqing and Shaanxi provinces, with the annual activity peak typically occurring around August. Infections caused by population mobility mainly occurred in hub cities with high connectivity and radiated to surrounding cities.

Conclusions: Findings from this nationwide study can help enhance situational awareness of the spread of JE and inform appropriate intervention strategies to advance the goal of JE elimination.

Introduction

Japanese encephalitis (JE) is a mosquito-borne viral disease caused by the Japanese encephalitis virus (JEV) that continues to be endemic throughout Southeast Asia, India, Indonesia, and parts of Australia.[1] JEV persists in the natural environment via a bird-mosquito cycle, but zoonosis may be enhanced via an intermediate pig-mosquito cycle, which brings the virus into closer contact with

* Corresponding author at: National Key Laboratory of Intelligent Tracking and Forecasting for Infectious Diseases, National Institute for Communicable Disease Control and Prevention, Chinese Center for Disease Control and Prevention, Beijing 102206, China.
** Corresponding authors.
E-mail addresses: liuxiaobo@icdc.cn (X. Liu), haoyt@bjmu.edu.cn (Y. Hao), pguo@stu.edu.cn (P. Guo).
[1] These authors contributed equally to this work.

https://doi.org/10.1016/j.jinf.2025.106609

humans.[1] Approximately 3 billion people are exposed to the risk of JEV infection in the world, and nearly 67,900 JE cases occur each year, resulting in 709,000 disability-adjusted life years annually.[2,3] Severe cases of JE generally have a poor prognosis, with one-third of infected people having neurological sequelae and one-third dying from the infection.[4] JE impairs the quality of life for patients and their families, placing a significant burden on global public health and the healthcare economy. In China, thousands of cases of JE are reported each year, with China accounting for 15.27% to 56.26% of all JE cases reported to the World Health Organization (WHO) during the period 2013–2018, displaying a significantly high disease burden.[5]

China has experienced sporadic JE outbreaks over the past decades, with remarkable spatial and temporal heterogeneity in disease distribution.[6] Despite widespread implementation of the JE vaccine and significant improvements in sanitation, the incidence is rising in China due to global warming and increased diagnostic capacity, as well as improved reporting awareness.[7,8] JEV continues to spread, especially in rural and peri-urban regions where environmental and socio-economic conditions favor its transmission.[9–12] The high incidence areas of JE are mainly distributed throughout southwestern and central China, such as Guizhou, Sichuan, Chongqing, and Henan provinces, which are greatly affected by climate and population density.[9] July to September is the primary epidemic season of JE, coinciding with the peak of the rainy season and the high incidence of mosquito activity.[13] Although previous studies have described environmental factors along with the spatiotemporal distribution of JE and quantified its associated burden in specific regions of China, these studies relied on small sample sizes of case surveillance data and were also geographically limited.[8,14–17] Therefore, they are unable to capture the dynamics of transmission that evolve over time or characterize the burden of JEV transmission across China. At present, there is a lack of research on the spatio-temporal transmission characteristics and burden of JE in China, and a comprehensive evaluation is urgently needed.

For a better understanding of the transmission of JEV and effectively control its future progression, it is essential to quantify the epidemiological characteristics of these outbreaks across both spatial and temporal scales. Therefore, we conducted a nationwide study on the epidemiology of JE using surveillance data of JE cases legally reported from the National Disease Notification and Surveillance System (NNDSS) covering 337 Chinese cities from 2013 to 2019. We adapted a city-resolved metapopulation network model[18] to simulate the spatio-temporal transmission of JE infection. This networked metapopulation model can flexibly generate complex population mobility patterns between different regions based on the observed inter-city population flow. Then, the metapopulation network integrates national surveillance data of JE cases and is coupled with the ensemble adjustment Kalman filter (EAKF), an iterative Bayesian inference algorithm, which assimilates weekly case observations across cities and intercity population movements.[18,19] The integration of the Bayesian inference technique facilitates the calibration of the model to case observations, enabling the parameters in the model to be updated iteratively, thus reducing the impact of unreasonable initial parameter setting and model error discretization.[20,21] At the same time, the method is also able to estimate hidden state variables, such as weekly new infections within a city, and time-varying parameters, such as time-varying transmission rates of the disease.[22] Therefore, we developed such a new method to simulate the evolution of transmission of mosquito-borne infectious diseases. This study represents the first attempt to comprehensively quantify the spatio-temporal transmission dynamics of JE in China and estimate the epidemiological burden caused by successive waves of JE epidemics to date.

Methods

Study domain

This study covered a total of 337 prefecture-level administrative divisions in China, including 293 prefecture-level cities, 30 autonomous prefectures, 7 counties and 3 leagues, and 4 municipalities. In order to make the analysis of regions consistent and easy to describe, administrative divisions at the prefecture, municipal and all other prefecture-level in the analytical framework were collectively referred to as 'city'. Therefore, a total of 337 cities (Fig. S1) were finally included in this study for descriptive analysis and simulation modeling of infectious disease transmission. In addition, these cities were further dynamically categorized into different city clusters according to the severity of JE epidemics in different years (Fig. S2 and Supplementary pp 15–17).

JE case surveillance data

All clinically diagnosed, laboratory-confirmed, and suspected cases of JE reported to the NNDSS of the Chinese Center for Disease Control and Prevention (China CDC) covering 337 cities from January 1, 2013, to December 31, 2019, were extracted. All cases of JE were diagnosed according to the diagnostic criteria issued by the Ministry of Health of the People's Republic of China (Criteria No. WS 214–2008).[23] The definitions of suspected, clinically diagnosed, and laboratory-confirmed cases of JE can be found in Supplementary pp 5–8. The diagnosis is based on a combination of epidemiological evidence, clinical presentation and laboratory findings of the patient. Information on JE cases included basic demographic information (age, sex, date of birth, national standard code of the individual's current residence, etc.), and time information on disease status (date of disease onset, date of diagnosis, and date of death). Further, the weekly number of JE cases was aggregated by individual current residential address to city-level spatial resolution for analysis. Each week was defined as a 7-day cycle that begins on January 1, resulting in a total of 52 weeks per year.

Mosquito abundance data and meteorological monitoring data

In this study, there were two types of mosquito abundance data, which were respectively used to assess the density of mosquito larvae and adult mosquitoes in each area. The Breteau Index (BI) was used as a quantitative indicator for assessing Aedes mosquito larval density.[18] Given that the primary vector of JEV is Culex tritaeniorhynchus, we calculated a weighted BI proposed by previous studies[24,25] to more accurately reflect the true mosquito vector density. The *BI* can be calculated by the following formula $BI = W \times (LPC/NH) \times 100$, where W represents the weight, LPC represents the number of positive containers (with Ae. aegypti pupae or larvae) inspected, and NH represents the number of households surveyed. Based on the mosquito abundance data of 89 monitoring sites across mainland China, *BI* values of each city were calculated. The adult Culex tritaeniorhynchus mosquitoes density was monitored using mosquito trapping lamps. In urban areas, monitoring sites were selected from three types of habitats, including residential areas, parks, and hospitals. In rural areas, two types of habitats, including residential houses and livestock sheds, were chosen. Monitoring was conducted twice per month throughout the entire annual mosquito population fluctuation cycle. Data on daily temperature (°C) during the period from January 1, 2013, to December 31, 2019, based on 2441 meteorological stations, was obtained from the China Meteorological Data Sharing System (http://data.cma.cn/). The ambient temperature data were matched to the respective cities

based on the geographical location of the stations. The average temperature for each city was calculated as the average temperature of meteorological stations within the city.

Population movement data

A metapopulation network model with inter-city population movement as the link was developed in this study to simulate the spatio-temporal transmission dynamics of JE infection. Initially, we obtained China's population movement statistics through the seventh population census in 2020, which is publicly released by the National Bureau of Statistics (http://www. stats.gov.cn/). In order to estimate city-level population migration data and match population outflows and inflows to our prefecture-level city administrations, we then obtained the weighting parameter (i.e., population migration index) representing the daily inter-city traffic volume from the Gaode Migration Big Data platform (https://trp.autonavi.com/ migrate/page.do). Based on location-based services (LBS), the Gaode platform collects geographic location changes from users' mobile phone positioning and describes the intensity of migration between cities. We further combined the population movement statistics of the census and the Gaode population migration index to derive weekly population migration flows between cities. Therefore, the weekly population migration inflows and outflows of people between different cities were calculated using the following formula $n_{A\leftarrow B}(t) = \rho_A \times \Sigma_{i=1}^{7} n_{A\leftarrow B}(t,i)/\Sigma_{k\neq A} n_{A\leftarrow k}(t,i))$, $t = 1{:}\ 52$. Here, $n_{A\leftarrow B}(t,i)$ is the migration index from city B to city A on week t and ρ_A denotes the static population inflow for city A according to the census. To reduce the potential impact of the COVID-19 pandemic on population migration patterns, we selected the human migration index for the entire year from June 1, 2018, to May 31, 2019, to match each calendar year. We assumed in the model that population mobility patterns were similar in each calendar year during the study period.

Stratification of urban and rural areas

We defined the main economic and population-dense areas of each prefecture-level city as urban areas, including 977 municipal districts, which typically have higher economic and educational levels and higher population density.[26] The remaining 1866 counties in each prefectural city were defined as rural areas, which are generally larger in area but have lower population density and economic level. To quantify the seasonal distribution of urban and rural JE cases across China, we developed a heatmap to describe the weekly number of JE cases during the entire year. In addition, to examine changes over consecutive years, a heatmap of the annual number of JE cases between 2013 and 2019 was also generated. According to the classification of urban and rural cases, we further used stacked bar charts to describe cases of different diagnostic categories. The study also revealed seasonal patterns in total cases, including urban and rural cases.

Latitudinal gradient characteristics of JE case distribution

Seasonal multiple linear regression models including time trends and reconciliation terms to represent annual and semiannual cycles[18,27–29] were also fitted to weekly time series of JE cases. Based on the estimated model coefficients, we extracted the amplitudes and peak times of the annual and semiannual cycles of the case count time series. The difference between the maximum and minimum values of the JE epidemiological curve is measured by the amplitude. The peak times referrs to the time point when the number of JE cases is at the highest level. In addition, the periodic information to describe the temporal spread of the disease considered in the model was mainly used to explore whether the epidemic cycle of JE appeared annually or semiannually.

Metapopulation network model coupled with Bayesian inference

The existence of cross-protective immunity against each genotype of the JEV in the population[30,31] is the basic assumption of the model constructed in this study. It also accounts for the widespread circulation of the five distinct JEV genotypes across various regions of mainland China.[32,33] Underpinned by these assumptions, we developed a dynamic compartmental model described by differential equations that encapsulates the transmission dynamics of JEV between mosquito vectors and human hosts. The basic idea is to divide the population and mosquitoes into several compartments to represent different disease states, and then use differential equations to study the transmission dynamics of JE. Therefore, the compartmental model ("*SI-SIR*" model) to study the propagation of JE was formulated which had five compartments. The part of vector compartments included susceptible (S_v) and infected (I_v) individuals, and the other part of human compartments included susceptible (S_h), infected (I_h), and removed (R_h) individuals, respectively. Therefore, the *SI-SIR* compartmental model,[18,19,34] incorporating the multi-host transmission mechanism encompassed both mosquito and human populations. The differential equations corresponding to the *SI-SIR* model are illustrated as follows:

$$\frac{dS_v}{dt} = -\frac{a_{vp}\beta_p I_p}{N_p} - \xi S_v + \varphi_b(t)(S_v + (1-U)I_v) - \varphi_d S_v$$

$$\frac{dI_v}{dt} = \frac{a_{vp}\beta_p I_p}{N_p} + \xi S_v + \varphi_b(t) U I_v - \varphi_d I_v$$

$$\frac{dS_h}{dt} = -\frac{\varepsilon\tau(t)\beta_h S_h I_v}{N_h}$$

$$\frac{dI_h}{dt} = \frac{\varepsilon\tau(t)\beta_h S_h I_v}{N_h} - \frac{I_h}{D}$$

Here, N_h denotes the total population size; N_p denotes the total number of pigs; a_{vp} represents the average bite rate of a mosquito on pigs; β_p is the probability of transmission of the virus from an infected pig to a susceptible mosquito; β_h is the probability of transmission of the pathogen from an infected mosquito to a susceptible person; ξ is the natural seeding rate of JEV in susceptible mosquitoes; $\varphi_b(t)$ and φ_d represent mosquito birth and death rates, respectively; U represents the vertical transmission probability of JEV in mosquitoes, which assumed to remain constant during the outbreak; and D is the average duration of transmission of the virus in humans. In order to forecast the spatial spread of JE cases, we further established a metapopulation model based on the differential equations of JEV dynamics, which can flexibly generate spatial spread patterns of JE cases and has proven to be advantageous in tracking widespread spatial transmission of infectious diseases.[18,22,35] In this model, special transmission patterns of reported cases (infected persons who have sought medical treatment and been reported) and unreported cases (asymptomatic infected individuals who have not sought medical treatment or not reported) have been set up to more accurately describe the actual transmission of JE in China. We hypothesize that, for reported cases, the likelihood of long-distance mobility is greatly reduced during recovery due to medical isolation or increased awareness of self-protection, and therefore mainly participation in limited local population interactions rather than participation in broader external population mobility.[36,37] In contrast, unreported asymptomatic infected people, who lack clear clinical symptoms or do not seek medical help, are often not included in the official case reporting system. We speculate that this group of people may participate in population movements between different regions in their daily lives just as healthy people do. In addition, since our model focuses primarily on interactions between human and mosquitoes, which typically do not migrate

over long distances due to their natural habits, the model additionally assumes that mosquitoes are confined to a single city from birth to death.

On the basis of the *SI-SIR* model, a city-resolved networked metapopulation model by the connectivity of inter-city population movements was constructed to simulate the spatio-temporal transmission of JEV. The model captured the dynamics of inter-city population movement through two modes of periodic commuters and random visitors.[18,37] The kind of periodic commuters can be further divided into three subgroups: healthy persons (N_{ii}^h) (those who both reside and work in location *i*), reported cases of infection ($\Sigma_{j\neq i} I_{ji}^{hr}(t)$) (those who reside in location *i* but work in location *j*), and unreported cases of infection ($\Sigma_{j\neq i}(N_{ij}^h - I_{ij}^{hr}(t))$) (those who work in location *i* but reside in location *j*). Thus, during the workday, the total population in location *i* can be calculated using the formula $N_i^{hw}(t) = N_{ii}^h + \Sigma_{j\neq i} I_{ji}^{hr}(t) + \Sigma_{j\neq i}(N_{ij}^h - I_{ij}^{hr}(t))$. Based on the aforementioned assumptions, when the susceptible mosquitoes (S_i^v) bite infected amplifying hosts such as pigs or migratory birds in location *i*, it gives rise to a new generation of infected mosquitoes (I_i^v). Subsequently, when these infected mosquitoes (I_i^v) come into contact with the susceptible population in location *i* at certain contact rate ($I_i^v(t)/N_i^{hw}(t)$), it creates a new generation of infected individuals. The number of human (I^{hp}) caused by periodic commuters can be respectively estimated as follows:

$$I^{hp} = \frac{\varepsilon_i(t)\tau_i(t)\beta_i^h(t)S_{ij}^h(t)I_i^v(t)}{N_i^{hw}(t)}$$

In the metapopulation network model, we considered not only the flow of periodic commuters, but also the flow of random visitors. We assumed that the number of people moving from city *j* to city *i* and randomly mixing with the population in city *i* was represented by $\theta dt_1 R_{ij}^h$. Furthermore, the probability that a random visitor was susceptible to infection was calculated using $\Sigma_k S_{jk}^h(t)/(N_j^{hw}(t) - \Sigma_k I_{jk}^{hr}(t))$, where $\Sigma_k S_{jk}^h(t)$ represented the number of susceptible individuals entering city *j* from all other city, and $(N_j^{hw}(t) - \Sigma_k I_{jk}^{hr}(t))$ represented the total number of floating population in city *j*, which was the total number of population minus that of reported infected individuals. Consequently, the total number of susceptible individuals entering city *i* was given by $\theta dt_1 \Sigma_{j\neq i} R_{ij}^h \Sigma_k S_{jk}^h(t)/(N_j^{hw}(t) - \Sigma_k I_{jk}^{hr}(t))$. Similarly, the number of susceptible individuals leaving city *i* was also calculated. The model assumed that the total number of population leaving city *i* was given by $\theta dt_1 N_{ji}^h$, and the figure of susceptible individuals was calculated using $\theta dt_1 \frac{S_{ij}^h(t)}{N_i^{hw}(t) - \Sigma_k I_{ki}^{hr}(t)} \Sigma_{j\neq i} R_{ji}^h$.

The calculation methods of random visitor flow in different compartments in the metapopulation model were similar. Since the model assumed that reported infected individuals and mosquitoes do not engage in long-distance movement, the compartments of report infected individuals and mosquitoes did not involve random movement. In addition, considering that the transfer of individuals between different compartments or the occurrence of infections can be regarded as sparse events, the Poisson distribution was used in this study to capture the randomness of these events. Therefore, we defined a single parameter ψ to estimate the average rate of occurrence of the event as follows:

$$P(X = k)\frac{\lambda^k e^{-\psi}}{k!}$$

where *k* is the number of occurrences. Therefore, Poisson distributed random sampling technique was used in the model to generate the dynamics of each compartment in order to better reflect the randomness and uncertainty of the real data of disease surveillance.

Then, the metapopulation network model integrated national surveillance data of JE cases and then coupled with the Bayesian inference-based EAKF algorithm, which assimilated weekly case observations and population movements of cross-city to iteratively update and estimate the parameters.[34] The main idea of EAKF was to use current observations to update the system state at a given time point.[21] When new JE observation data entered the model, the algorithm used these observation data to update the observed state variables and iterated continuously until a set time point was reached. The EAKF can run a series of assimilation cycles, each consisting of a model prediction and a filter update, to perform sequential data assimilation and constantly update state variables and parameters within the state space.[35] As time progresses, more and more data of JE cases are added to the process of state parameter updating and model optimization, which theoretically enables this metapopulation network model to better capture epidemics of different scales in different regions.[38] This method has been successfully applied to infer the epidemiological parameters of different infectious diseases.[34,39] Details of this model are described in the Supplementary pp 8–14.

Inference of JE transmission dynamic parameters

Three parameters including the mosquito-to-human transmission rate (β_{mth}), the effective reproduction number (R_{eff}) and the force of infection (F_{inf}) parameter,[18,40] were adopted to reveal the transmission dynamics of the pathogen in our study. The R_{eff} is a basic indicator that represents the secondary cases produced by one typical infection with JE joining in a population during its infectious period. The F_{inf} signifies the probability of a susceptible individual contracting JEV, contingent upon the likelihood of acquiring the virus from an infected mosquito. These parameters can reveal the potential transmission dynamics of the pathogen and help to formulate more effective prevention and control measures to reduce the risk of JE transmission. Specifically, the mosquito-to-human transmission rate of the pathogen in city *i* is defined as follows:

$$\beta_{mth} = \varepsilon(t)\tau_i(t)\beta_i^h(t)$$

where $\varepsilon_i(t)$ denotes the weekly adjusted transmission rate estimated by the model for each city, $\tau_i(t)$ represents the mosquito biting rate, and $\beta_i^h(t)$ is the probability of transmission of the pathogen from vectors to humans. Furthermore, in order to reveal the dynamic characteristics of the pathogen in each city, the weekly time series of R_{eff} and F_{inf} were also calculated using the following formula:

$$R_{eff} = R_0\sqrt{\frac{S_i^h(t)S_i^v(t)}{N_i^h N_i^v}} = \sqrt{\frac{\varepsilon_i^2(t)\tau_i^2(t)\beta_i^h(t)S_i^v(t)S_i^h(t)D}{(\varphi_d - \varphi_b(t)U)(N_i^h(t))^2}}$$

$$F_{\inf(t)} = \frac{\varepsilon_i(t)\tau_i(t)I_i^v(t)\beta_i^h(t)}{N_i^h(t)}$$

where $S_i^h(t)$ is the total number of susceptible individuals at a location *i* at time *t*. It is the sum of the number of susceptible individuals $S_{ii}^h(t)$ residing at the location and the number of susceptible individuals $S_{ik}^h(t)$ coming to that location from other locations k($k\neq i$). The $N_i^h(t)$ was calculated as follows:

$$N_i^h(t) = N_{ii}^h(t) + I_{ik}^h(t) + S_{ik}^h(t)$$

where $N_i^h(t)$ represents the total population at location *i* at time *t*, $N_{ii}^h(t)$ represents the reported infected individuals residing at location *i*, $I_{ik}^h(t)$ represents the number of reported infected individuals from locations $k(k\neq i)$ who came to that location for daily commuting, and $S_{ik}^h(t)$ represents the reported susceptible individuals who came to that location from location *k*.

Moreover, we assessed the relationship between JE epidemic intensity and the size of population movement. We estimated the number of JE cases caused by population movements using the following formula:

$$I_{pm} = I^{hr} + I^{hu} - I_{ii}^{hr} - I_{ii}^{hu}$$

where I_{pm} represents the number of infections caused by population movement in each city, I^{hr}+I^{hu} represents the total number of infections (including the number of reported I^{hr} and unreported cases I^{hu}), and I_{ii}^{hr} represents the number of infections caused by local commuters (including the number of reported I_{ii}^{hr} and unreported cases I_{ii}^{hu}).

Results

Spatial-temporal distribution and seasonal characteristics of JE

Our study included a total of 9061 reported JE cases from 337 cities in China between 2013 and 2019. With 10 cases missing municipal residential addresses and 56 cases outside the cities included, 8995 cases were used for data analysis. In order to investigate the distribution difference of JE in urban and rural areas, cases were divided into three categories including urban cases, rural cases and total cases. We found that the number of cases was greatly higher in rural (n=7089) than urban areas (n=1911). The annual epidemic peak of JE generally occurred between June and October, with sporadic cases occurring the rest of the year. In terms of spatial distribution, there was a spatial delay in the occurrence of JE epidemic peak in China, showing that the north was later than the south (Fig. 1A, B). Similar spatial and temporal patterns of JE epidemics were observed in rural and urban areas (Fig. 1D, E, G, H). The number of JE cases initially dropped from a peak in 2013 to a nadir in 2015, then rebounded to another peak in 2018, and subsequently fell to a new low in urban areas in 2019 (Fig. 1C, F, I). In China, JE cases were predominantly concentrated in central provinces such as Sichuan, Chongqing and Shaanxi during the 7-year study period (Fig. S1, S2). Among the reported JE cases, the majority were laboratory-confirmed (82.53%, n=7478), followed by clinically confirmed cases (9.56%, n=866) and suspected cases (7.91%, n=717) (Fig. 1C, F, I).

Fitted seasonal models of JE cases by each province were preserved in Figs. S3-S6. Nationwide, the JE cases exhibited an annual peak of activity, typically peaking around August. The timing of the annual peak of JE epidemics, however, varies apparently across different provinces (p-value < 0.05), with the peak in the southern region around the 30th week, the central region around the 33rd week, and the northern region around the 37th week, respectively (Fig. 2B, E). There was no significant difference (p-value > 0.05) in the annual amplitude fluctuations of JE epidemic across different provinces (Fig. 2A, D). In addition, the semi-annual periodicity of JE did not differ significantly across latitudes (p-value > 0.05) (Fig. 2C, F). Similarly, no significant differences were observed across longitudes (Fig. S7).

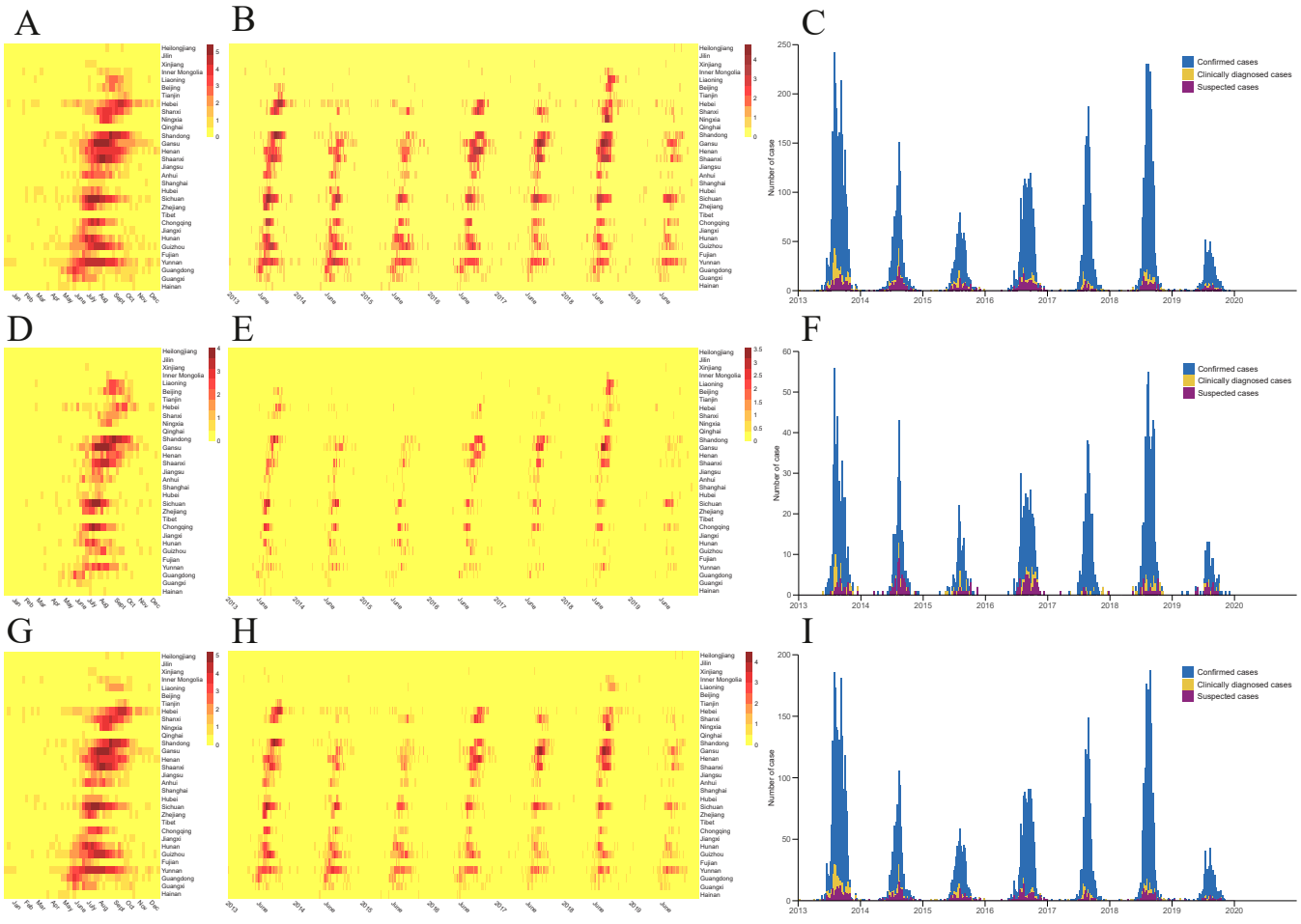

Fig. 1. Spatial and temporal distribution of cases of Japanese encephalitis, 2013–2019. Seasonal distribution of national (A), urban (D), and rural (G) Japanese encephalitis cases plotted as weekly cases throughout 2013–2019. Weekly time series of national (B), urban (E), and rural (H) Japanese encephalitis cases, transformed to annual case counts. In the above heat map, these provinces are sorted by latitude from northernmost (top) to southernmost (bottom) and the number of cases is log-transformed. Time series of weekly cases of Japanese encephalitis from nationwide (C), urban (F) and rural (I) areas are shown, grouped by probable, laboratory-confirmed and clinically diagnosed cases.

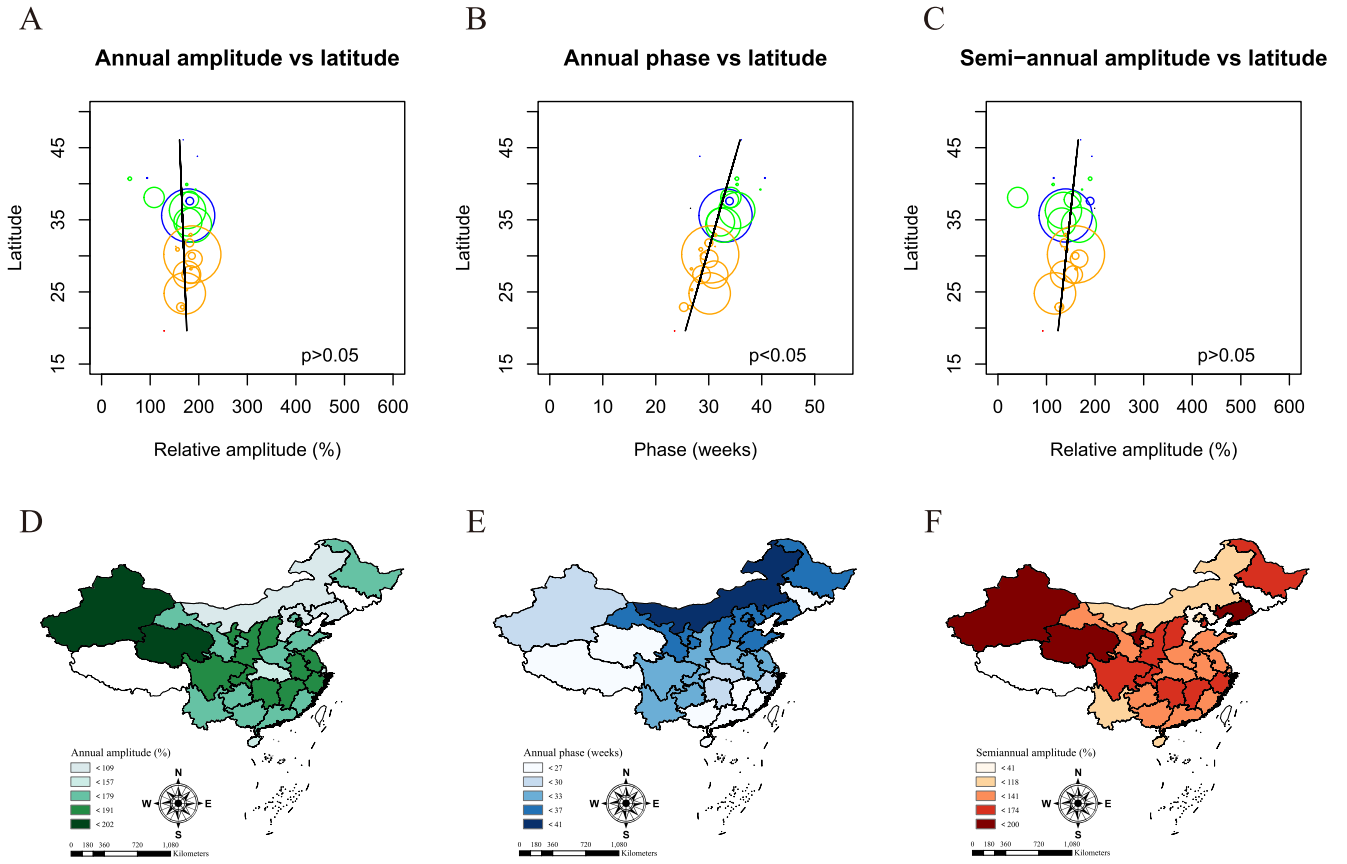

Fig. 2. Characteristics of the latitudinal gradient of the epidemic cycle and peak time of Japanese encephalitis in China. (A) Annual period amplitude. (B) Time of the main peak of Japanese encephalitis per year. (C) Amplitude of the half-yearly cycle. Colors represent different climatic zones (red = tropical, yellow = subtropical, green = warm temperate, blue = middle temperature, black = cold temperate). Symbol size is proportional to the number of cases of Japanese encephalitis in each province. The solid black line indicates the result of a linear regression fit (regression results weighted by the annual average number of Japanese encephalitis cases). *P*-values of statistical tests are shown in the figure. (D) Annual period amplitude by province. (E) Timing of major annual peaks of Japanese encephalitis in each province. (F) Amplitude of the half-yearly cycle in each province.

Inherent dynamics of JEV spread

By fitting the inferred transmission model of the JE to weekly observed case data, we successfully estimated the magnitude of outbreaks in three urban clusters as well as nationwide. These findings were presented in Fig. 3. At the national level, the model inference results were highly accurate during the simulated period, with the median model-fit ensemble closely matching the observed number of cases and the 95% confidence intervals (CIs) covering nearly all observations (Figure 3A1-A5). Similarly, in Region 1, the model performed excellent as well up to week 31, with the majority of cases captured and encompassed by the 95% CI (Figure 3B1-B5). In Region 2, the model's performance stayed robust up to Week 29, accurately forecasting both the timing and the scale of the outbreak, with 95% CIs catching most observed cases (Figure 3C1-C5). In Region 3, the model also precisely forecasted the timing of the peak at all instances (Figure 3D1-D5). We also estimated the number of monthly infections nationwide in 2018 (Figure 3E1-E5). The total number of estimated JE infections in China peaked in August, with 1348 (95% CI: 1260 - 1569) new infections during the month. In addition, we compared the estimated number of infections in the three urban agglomerations in 2018 with the actual number of infections (Figure 3F1-H5). For Region 2, the highest number of infections was estimated for August, with 967 cases (95% CI 870–1195) in Week 29. In general, the number of infections in various regions and the corresponding dynamic transmission parameters began to rise in June, reached a peak around August and September, and then progressively dropped to zero.

Then, we focused on the changes of dynamic transmission parameters of JE in the three major urban agglomerations, as illustrated in Fig. 4. In these urban agglomerations, the dynamic change trend of JE parameters was generally consistent, especially for the parameters β_{mth} and R_{eff}. Around the 31st week, the β_{mth} values of JE peaked, and gradually decreased to near zero after the 35th week in Region 1 and Region 2, respectively (Fig. 4 A-B). Similarly, the β_{mth} in Region 3 peaked around the 29th week to the 35th week (Fig. 4C). The values of R_{eff} of JE epidemics varied among different agglomerations, but similarly, the parameter rose gradually at first, reached a peak, then began to decline, and finally approached zero (Fig. 4D-F). The values of F_{inf} of JE transmission in the three areas were low and increased only slightly during the critical epidemic period (Fig. 4G-I). We also estimated the number of infections in the three major urban clusters (Table 1) and all the cities covered (Table S3). Besides, the results of the inferred parameter including β_{mth}, R_{eff} and F_{inf} for these regions were presented in Table 1 and Table S3.

We identified the main epidemic weeks of JE infections in each city and how the R_{eff} varied across cities (Fig. 5). The estimated cases of JE infection mainly concentrated in central China during the 29th week. After 2 weeks, the estimated infections gradually spread from central to southern and northern regions. In central China, JE infections peaked in week 33 and subsequently showed a downward trend (Fig. 5A-F). We further depicted the relationship between the intensity of population mobility in city networks and the number of infections due to population mobility (Fig. 5G-L). Infections caused by population mobility mainly occurred in hub cities with large population mobility and radiated to surrounding cities. Being able to identify high-risk periods

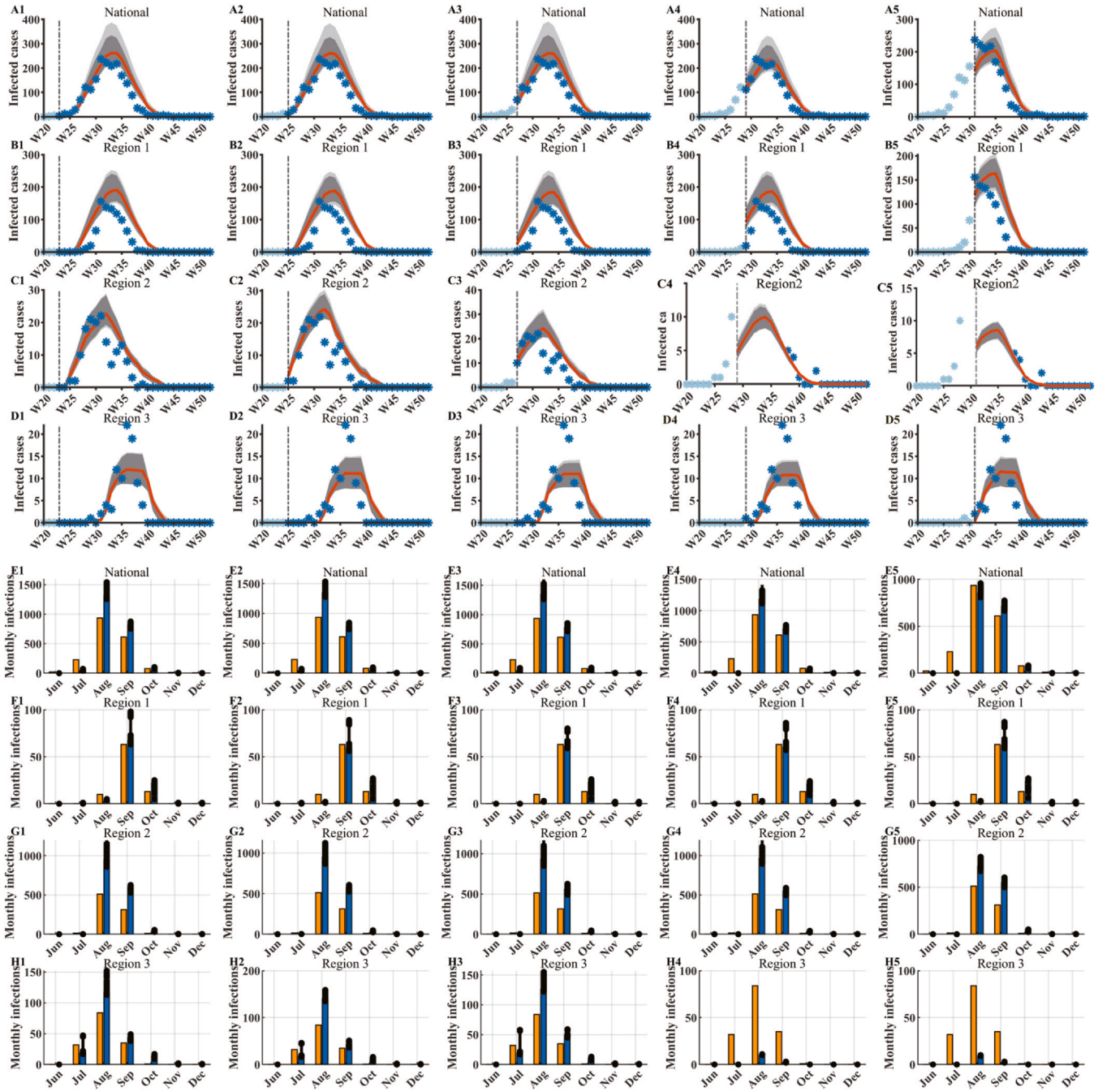

Fig. 3. Model fitting and estimation of national Japanese encephalitis infection. (A1-D5) Model fit for the weekly number of Japanese encephalitis cases (blue plus signs) in China as a whole and in three city clusters. The solid red line represents the median of the estimates. The dashed black line indicates the number of weeks at which the model started to fit. Shaded dark and shaded light intervals indicate corresponding 99% and 95% confidence intervals (CIs) of the estimates, respectively. (E1-H5) Monthly actual number of confirmed cases (orange bars) and estimated number of infections (blue bars) of Japanese encephalitis in the whole country and three city clusters, respectively. Distribution is obtained from 300 ensemble members generated by the coupled model. Blue bars represent the medians derived from this distribution, and whiskers represent the 95% CIs, respectively.

and areas during an epidemic, changes of R_{eff} are essential for characterizing the intrinsic transmission dynamics of JEV. Cities with higher values of R_{eff} were concentrated in central China, especially in the Sichuan and Chongqing regions. The R_{eff} parameter began to rise at 29 weeks, peaked around 33 weeks, and then gradually declined to near zero (Fig. 5M-R). It was seen that cities with higher values of R_{eff} predominantly overlapped with these hubs (Fig. 5G-L), substantiating the significance of human mobility in facilitating the geographical dissemination of JE, especially in regions with high connectivity.

Comprehensive sensitivity analyses demonstrated robust model inference across the parameter space, with consistent output patterns observed under varying scenarios (Figs. S8-12). We also fitted models to actual data on JE cases to respectively estimate the total number of infections per month for the period from 2013 to 2017 and 2019 alone (Figs. S13-15). Results revealed inter-annual fluctuations in JE epidemic magnitude between 2013 and 2017 and 2019 alone, while maintaining comparable seasonal activity patterns across years (Figs. S13-15).

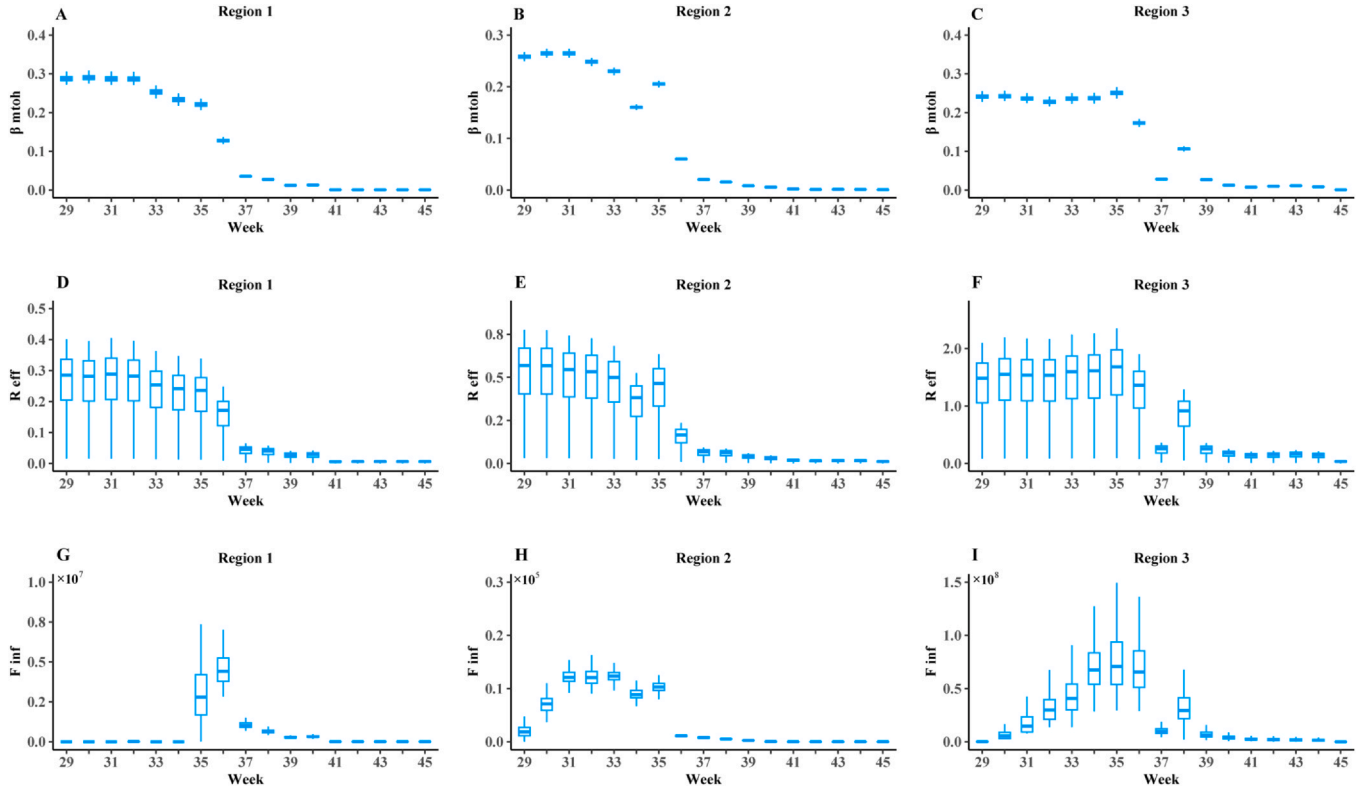

Fig. 4. Inference of time-varying transmission parameters for Japanese encephalitis in three regions. (A-C) Distribution of transmission rates for Japanese encephalitis. (D-F) Distribution of effective reproduction numbers for Japanese encephalitis. (G-I) Distribution of force of infection for Japanese encephalitis. The center line indicates the median, the box boundary denotes the inter-quartile range, and the dashed line represents the range, respectively. Distribution is obtained from 300 ensemble members generated by the coupled model.

Discussion

This study analyzed more than 9000 cases of JE reported in 337 cities in China from 2013 to 2019, revealing the geographic distribution, temporal dynamics and transmission characteristics of JEV, and further comprehensively quantifying the national burden. During the study period, the number of JE cases experienced a dynamic trend characterized by a decline from a peak to the lowest, followed by a gradual rise to another peak. The geographic distribution of cases was expanding but predominantly concentrated in central China, with the epidemic showing a delayed progression from south to north. Our large-scale study, covering 337 distinct cities in China, demonstrates that although the peak time of JE outbreaks varies among provinces, the annual peak usually occurs between August and September. The magnitude of the annual epidemic does not vary significantly with latitude or longitude. Coupled

Table 1
Parameter estimates for three major regions derived from the disease transmission dynamics model.

Region	City	Effective reproduction number	Transmission rate	Force of infection
Region 1	Tianshui	1.0115 (0.9905, 1.0324)	0.2355 (0.2348, 0.2362)	7.2069e-06 (7.1700e-06, 7.2437e-06)
	Longnan	0.9298 (0.9104, 0.9491)	0.2437 (0.2429, 0.2444)	7.7861e-06 (7.7570e-06, 7.8152e-06)
	Pingliang	0.564 (0.5524, 0.5757)	0.2061 (0.2055, 0.2068)	6.0725e-06 (5.8697e-06, 6.2753e-06)
	Yinchuan	0.1441 (0.1411, 0.1472)	0.2652 (0.2638, 0.2667)	1.6315e-06 (1.4717e-06, 1.7913e-06)
	Qingyang	0.4063 (0.3979, 0.4147)	0.2181 (0.2175, 0.2187)	2.0583e-08 (1.9564e-08, 2.1601e-08)
	Yan'an	0.225 (0.2203, 0.2297)	0.2433 (0.2425, 0.2441)	5.1532e-09 (4.7116e-09, 5.5948e-09)
	Baoji	0.6867 (0.6725, 0.7010)	0.2823 (0.2815, 0.2831)	4.9676e-06 (4.8034e-06, 5.1319e-06)
	Shizuishan	0.1237 (0.1211, 0.1263)	0.2518 (0.2502, 0.2534)	3.7198e-06 (3.3542e-06, 4.0854e-06)
	Xianyang	0.5622 (0.5506, 0.5739)	0.2956 (0.2949, 0.2964)	2.4363e-08 (2.3422e-08, 2.5304e-08)
	Luoyang	0.959 (0.9392, 0.9788)	0.2933 (0.2925, 0.2942)	2.0904e-09 (1.9252e-09, 2.2556e-09)
	Yuncheng	0.4212 (0.4125, 0.4299)	0.2885 (0.2877, 0.2893)	1.7162e-09 (1.5141e-09, 1.9183e-09)
	Wuzhong	0.1209 (0.1184, 0.1235)	0.2418 (0.2406, 0.2430)	2.8970e-08 (2.6196e-08, 3.1743e-08)
	Weinan	0.3405 (0.3334, 0.3476)	0.2966 (0.2958, 0.2973)	5.7775e-09 (5.3604e-09, 6.1946e-09)
Region 2	Chongqing	2.8891 (2.8283, 2.9499)	0.2603 (0.2578, 0.2627)	2.1287e-09 (2.0153e-09, 2.2420e-09)
	Zunyi	0.7558 (0.7401, 0.7714)	0.2774 (0.2762, 0.2786)	5.0289e-10 (4.2240e-10, 5.8338e-10)
	Zhaotong	1.3981 (1.3686, 1.4276)	0.2317 (0.2300, 0.2335)	2.0384e-10 (1.3865e-10, 2.6903e-10)
	Liangshan Yi Autonomous Prefecture	0.466 (0.4561, 0.4759)	0.17 (0.1689, 0.1710)	3.4410e-10 (2.7515e-10, 4.1304e-10)
Region 3	Panjin	0.1472 (0.1442, 0.1502)	0.2912 (0.2904, 0.2920)	4.2568e-10 (2.5666e-10, 5.9470e-10)
	Beijing	0.2334 0.2286, 0.2382)	0.2811 (0.2804, 0.2818)	8.4220e-10 (7.7093e-10, 9.1347e-10)
	Taian	0.388 (0.3799, 0.3960)	0.2895 (0.2889, 0.2902)	2.4006e-10 (1.6136e-10, 3.1877e-10)

The weekly average of estimated effective reproduction number, transmission rate, and force of infection around peaking time from the 29th week to the 32th week in 2018 based on the proposed model. The median and corresponding 95% confidence intervals (CIs) of the estimated parameters are displayed. Distribution is obtained from 300 ensemble members generated by the coupled model.

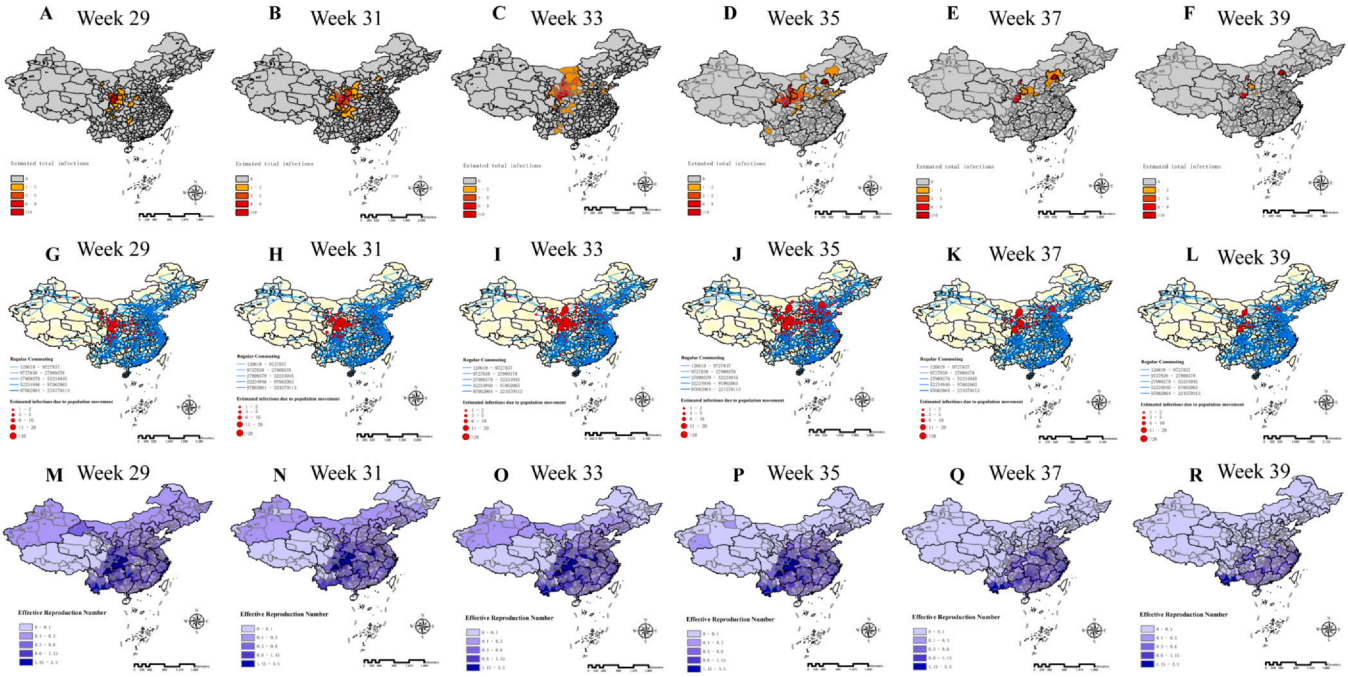

Fig. 5. Relationship between human mobility and spatiotemporal spread of Japanese encephalitis and estimated effective reproduction numbers for 337 cities across the country based on the model. (A-F) Estimated total weekly number of individuals infected with Japanese encephalitis in each city. Redder colors in the cities indicate more severe infections, and the legend records the specific range of numbers infected. (G-L) Estimated number of infections due to population movement per city and the inter-city network of population movement intensity. The red dots represent the number of infections in a city, with larger dots indicating a larger number of infections. The thickness of the blue line represents the intensity of population movement between cities. (M-R) Weekly estimates of the effective reproduction numbers of Japanese encephalitis in each city during the peak and post-peak epidemics period. Purple shading represents the magnitude of the effective reproduction numbers and gray shading represents no extrapolation, respectively.

with an iterative Bayesian inference technique, a networked metapopulation model was developed to successfully simulate the transmission trajectory of JEV across 337 cities in China. Our study demonstrated that the proposed model can accurately predict the scale and peak time of the seasonal epidemic of JE, and successfully infer the dynamic parameters of its seasonal transmission in China.

As a nationwide population-based study on the spatiotemporal dynamics of JE transmission, our study enhances the understanding of the mechanism and dynamic characteristics of mosquito-borne disease transmission across both time and geographical scales. We found that JE cases in China were particularly concentrated in central provinces such as Sichuan and Chongqing, which was consistent with previous findings.[33] The spatiotemporal distribution pattern of JE cases in urban and rural areas remained largely consistent, which also reflected the delay of the northward spread of JE epidemic peak. The epidemic peak of JE appeared earlier in southern China, followed by central regions and finally northern regions, indicating that the transmission dynamics of JE in different environments had certain commonality.[41] Notably, our study found that the number of JE cases in rural areas of China was much higher than in urban areas, especially in areas engaged in rice cultivation and flood irrigation.[42,43] This may be explained by the fact that rice fields in these areas not only serve as breeding grounds for Culex mosquitoes but also attract migratory birds that participate in the transmission cycle. Moreover, the widespread distribution of pig farms in rural areas increases the probability of virus-carrying mosquitoes biting pigs and humans, thus increasing the risk of JE transmission among local residents.[44] Pigs serve as key amplification hosts for JEV to enhance viral transmission dynamics, therefore, our modeling framework incorporated their amplifier function through mosquito-people interaction. Besides, we also acknowledge that the vaccination status of human JE vaccines has an impact on the transmission of JE. However, our model did not take the vaccination factor into account. This is mainly because we simulate the spatio-temporal transmission of JE infection based on a city-resolved metapopulation network model, which has complex parameters and hyperparameters. If the status of human vaccination against JE is further considered, the compartment model with the SI-SIR structure needs to be expanded. Given that the primary objective of this study focused on inferring key transmission parameters of JE, incorporating this factor in the model will make the model extremely complex, thus reducing the reliability of parameter inference.

The epidemic of the JEV exemplifies the influence of human mobility on epidemic spreading. To study the dynamics of JE transmission, networked metapopulations provide a valuable modeling framework that takes into account the heterogeneous flow of humans. The metapopulation model proposed in our study used census data and population migration index based on location-based services describing the migration intensity to track the movement of individuals between cities. The population mobility data and other data streams were functionally compartmentalized within our modeling framework, and each data stream played a unique role in the construction of transmission dynamics model. By integrating an iterative Bayesian inference algorithm with disease transmission dynamics models, the interconnected metapopulation network successfully simulated the transmission dynamics of JE across the country and in three urban agglomerations and revealed the scale of JE outbreaks at the national and major urban agglomeration levels. In order to reveal the transmission dynamics of JEV in China, several indicators including R_0 and R_{eff} derived from the metapopulation network model, were estimated. R_0 is crucial in the early stages of an epidemic because it represents the expected number of secondary infections from an infected person in a susceptible population in the absence of any preventive measures.[45] While R_{eff} incorporates factors such as the immune status of populations, intervention measures (e.g., vaccination), and other variables that may influence transmission, thereby reflecting the actual transmission capacity under real situation.[46] R_{eff} and peak timing are essential for targeted

measures in JE prevention and control as they identify high-risk periods and areas during an epidemic.[47] According to our findings, high R_{eff} values were primarily concentrated in central regions, further confirming these areas as core regions for JE transmission. The results showed the seasonality of JE transmission dynamics, with R_{eff} rising peaking around August and gradually declining in September, which also aligned with previous studies.[48–50] The variations of R_{eff} and infection force for JE across cities in nationwide China have been demonstrated as well (Table S3). Among the three urban agglomerations, the R_{eff} in region 1 and region 2 consistently remained below 1, with only a slight increase during the peak period, approaching zero at the other time. In region 3, R_{eff} exceeded 2 during the outbreak period, driving the transmission of JE. This finding underscores the need to develop precise intervention strategies in areas of high epidemiological susceptibility to lay the groundwork for effective containment of mosquito-borne diseases.

Accordingly, the advanced economic growth and convenient population mobility in the modern era has made population mobility become another potential trigger for mosquito-borne diseases.[51,52] Individuals traveling from endemic areas may carry the virus to non-endemic regions, and when JEV is introduced into immunologically naive populations, clinical disease can manifest across all age groups, consequently increasing the risk of localized outbreaks, particularly in regions characterized by low vaccination coverage or inadequate vector control measures.[43] Therefore, it is imperative to construct a refined population mobility network to elucidate the disease burden of JEV attributable to human movement. Considering each city as a subpopulation, our metapopulation network model covering 337 cities enables us to accurately capture the impact of human mobility on the transmission dynamics of JEV. The movement of people partly explained JEV's delayed progression from south to north in China that we described earlier. Infections driven by population movement primarily occur in hub cities with high population movement in Chinese central areas, subsequently radiating to neighboring cities. In addition, the results of R_{eff} showed that cities with higher R_{eff} values largely coincided with these hubs, which strengthens the role of population movement in the spatial propagation of JE, particularly in regions with high connectivity. Our findings revealed that hubs act as critical nodes in viral transmission networks, shaping the dynamics of disease spread - a pattern that was largely consistent with the "gravity models" in epidemiology.[53,54] These crucial findings could be leveraged to provide technical assistance before and during the infectious mosquito-borne disease outbreaks, guiding the establishment of diagnostic networks for virus transmission. By identifying and monitoring key transmission hubs, real-time updates and iterative improvements can be made for the management of mosquito-borne disease.[55] More in-depth researches are encouraged to build upon these insights by integrating flexible population mobility data into a networked system that both supervises and diagnoses, thereby strengthening national defenses against more mosquito-borne infectious diseases. However, the observed incidence pattern of JE cannot be solely explained by population mobility, the high incidence in some non-hub cities (e.g. the Shaanxi-Gansu-Ningxia region) may be the result of the interactions of multiple factors, especially for the local agricultural ecological characteristics and other factors.[33]

The traditional compartmental "SIR" model uses ordinary differential equations to simulate the transition from "susceptible" to "infected" to "recovered" states. However, traditional compartmental infectious disease models often struggle to capture the complexity of high-dimensional systems, accompanied by limitations such as discrete prediction errors and high sensitivity to initial conditions.[56,57] In addition, these models lack the flexibility to account for the complex and rapidly changing transmission dynamics of pathogens. Our prior researches implemented the iterative Bayesian inference algorithm-EAKF-to mitigate the sensitivity of traditional compartmental models to initial parameter values and address the adverse effects of zero-inflated data distributions on modeling, enabling accurate inference of disease transmission parameters and burden across both temporal and spatial scales.[35,39] Taking both human and mosquito compartments into consideration, we developed mathematical models of JEV transmission based on a system of differential equations, featuring a sequence of high-dimensional parameter vector ($V = \{S(t), I(t), R(t)... \alpha, \beta, \lambda\}$). The EAKF was applied to assimilate weekly JE case observations from each city and intercity population mobility. By fitting the model to case observations using the Bayesian inference technique, unobserved state variables and system parameters were iteratively calibrated and estimated. The sensitivity analysis in our study demonstrated a robust estimation of the spread of JEV over a wide range of initial model conditions, proving the robustness of this method to parameter perturbations (Fig S8-S12). Our results indicate that the developed model can accurately fit the observed JE case data, capturing the consecutive epidemic waves occurring at both the national and city levels.

As a nationwide study, our research achieved some advances in elucidating transmission dynamics of JEV. By coupling with the EAKF algorithm, this study overcomes the limitations of the traditional compartmental models of infectious disease, we inferred transmission parameters precisely on a spatiotemporal scale. A refined metapopulation network model covering 337 cities was developed to quantify the role of population migration in the transmission of JEV in China. The established model naturally integrated population immunity and iteratively estimated the time-evolving parameters of R_{eff}, which was helpful for evaluating the effectiveness of vaccines or other public health intervention measures. Furthermore, the integration of multi-dimensional data enabled us to simulate JEV transmission at national and urban agglomeration scales, which identified high-risk regions, thus improving the situational awareness capabilities for mosquito-borne diseases. We bridged gaps in JEV dynamic modeling, offering transformative tools for public interventions of mosquito-borne diseases. Despite the progress we made, the study still has several limitations. Although our analysis utilized mosquito vector abundance data from 89 surveillance sites, representing the most comprehensive surveillance information currently available nationwide, limited accessibility in some remote areas may lead to potential bias in our density estimates. Second, our research examined the spread of JE based on large-scale population mobility between cities. But our study could not discern finer details, such as how far individuals traveled, how long they spent in different concrete locations, or how often they visited different destinations. Third, the pathogen of JEV in China is predominantly represented by genotype I (GI) and III (GIII), featuring discrepant transmission cycles and dynamics.[58] Considering the heterogeneity of virus transmission among populations in different cities, our study did not take into account the clade-specific effects of GI and GIII on transmission dynamics. Future studies should further explore the differences in transmission modes between the two genotypes.

Conclusions

In summary, this study comprehensively quantified the evolution of the time-evolving epidemiological characteristics of JE in China from 2013 to 2019. The integration of networked metapopulation and Bayesian inference method expands the understanding of dynamic transmission of JE at temporal and spatial scales, providing empirical evidence for identifying high-risk populations susceptible to mosquitoes and implementing prevention strategies. Our work

enhances the situational awareness of the spread of mosquito-borne diseases, on which future mitigation policies can consider building early warning systems for mosquito-borne diseases.

Author contributions

XYC, XW, HBN, and JYZ contributed to conceptualisation, formal analysis, methodology, software, validation, visualisation, writing-original draft, writing-review and editing. XBL contributed to conceptualisation, data curation, funding acquisition, investigation, project administration, writing-review and editing. YTH, and PG contributed to conceptualisation, formal analysis, data curation, methodology, project administration, writing-review and editing. YL, and XYF contributed to data curation, investigation, and validation. YCY, TTD, LXW, LF, YC, YYW, BW, WNZ, RHZ and SP contributed to data curation, validation, and writing-original draft. All authors read the manuscript, provided feedback, and approved the final version. XBL, YTH, and PG had final responsibility for the decision to submit for publication.

Data availability

Japanese encephalitis surveillance data are available at the National Notifiable Disease Surveillance System of the Chinese Center for Disease Control and Prevention. To access these data and/or to seek permission for their use, please contact the Data Center of China Public Health Science (https://www.phsciencedata.cn/Share/index.jsp) or email data@chinacdc.cn. All other data utilized in this study were accessed from open sources. Meteorological data were obtained from the China Meteorological Data Sharing System (http://data.cma.cn/). Demographic and mobility data were collected from China's seventh census in 2020, which can be publicly obtained from the National Bureau of Statistics of China (http://www.stats.gov.cn/). The population migration data at daily city-level was obtained from the platform of Gaode Migration Big Data (https://trp.autonavi.com/migrate/page.do).

Declaration of Competing Interest

The authors declare that they have no known competing financial interests or personal relationships that could have appeared to influence the work reported in this paper.

Acknowledgments

This work was supported by the Consultancy Project by the Chinese Academy of Engineering (No. 2023-JB-12). We appreciate the efforts of the staff at the hospitals, local health departments, and municipal-, provincial-, and national- level Centers for Disease Control and Prevention in the data collection process.

Appendix A. Supporting information

Supplementary data associated with this article can be found in the online version at doi:10.1016/j.jinf.2025.106609.

References

1. Barrows NJ, Campos RK, Liao KC, Prasanth KR, Soto-Acosta R, Yeh SC, et al. *Biochemistry and molecular biology of flaviviruses. Chem Rev* 2018;**118**(8):4448–82.
2. Xu C, Zhang W, Pan Y, Wang G, Yin Q, Fu S, et al. *A bibliometric analysis of global research on japanese encephalitis from 1934 to 2020. Front Cell Infect Microbiol* 2022;**12**:833701.
3. Bharucha T, Shearer FM, Vongsouvath M, Mayxay M, de Lamballerie X, Newton PN, et al. *A need to raise the bar—a systematic review of temporal trends in diagnostics for Japanese encephalitis virus infection, and perspectives for future research. Int J Infect Dis* 2020;**95**:444–56.
4. Im J, Balasubramanian R, Yastini NW, Suwarba IGN, Andayani AR, Bura V, et al. *Protecting children against Japanese encephalitis in Bali, Indonesia. Lancet* 2018;**391**(10139):2500–1.
5. Wu D, Chen X, Liu W, Fu S, Li F, Liang G, et al. *Emergence of Japanese encephalitis among adults 40 years of age or older in northern China: epidemiological and clinical characteristics. Transbound Emerg Dis* 2021;**68**(6):3415–23.
6. Li X, Gao X, Ren Z, Cao Y, Wang J, Liang G. *A spatial and temporal analysis of Japanese encephalitis in mainland China, 1963-1975: a period without Japanese encephalitis vaccination. PLoS One* 2014;**9**(6):e99183.
7. Bello MB, Alsaadi A, Naeem A, Almahboub SA, Bosaeed M, Aljedani SS. *Development of nucleic acid-based vaccines against dengue and other mosquito-borne flaviviruses: the past, present, and future. Front Immunol* 2025;**15**:1475886.
8. Deng X, Yan R, Li ZQ, Tang XW, Zhou Y, He H. *Economic and disease burden of Japanese encephalitis in Zhejiang Province, 2013-2018. PLoS Negl Trop Dis* 2021;**15**(6):e0009505.
9. Wang L, Hu W, Soares Magalhaes RJ, Bi P, Ding F, Sun H, et al. *The role of environmental factors in the spatial distribution of Japanese encephalitis in mainland China. Environ Int* 2014;**73**:1–9.
10. Li F, Li H, Yang L, Wang L, Gu L, Zhong G, et al. *The spatial-temporal pattern of Japanese encephalitis and its influencing factors in Guangxi, China. Infect Genet Evol* 2023;**111**:105433.
11. Liu MD, Li CX, Cheng JX, Zhao TY. *Spatial statistical and environmental correlation analyses on vector density, vector infection index and Japanese encephalitis cases at the village and pigsty levels in Liyi County, Shanxi Province, China. Parasit Vectors* 2022;**15**(1):171.
12. Tu T, Xu K, Xu L, Gao Y, Zhou Y, He Y, et al. *Association between meteorological factors and the prevalence dynamics of Japanese encephalitis. PLoS One* 2021;**16**(3):e0247980.
13. Zheng P, Wen Z, Liu Y, Wang Q. *The spatiotemporal distribution and prognostic factors of Japanese encephalitis in Shanxi Province, China, 2005-2022. Front Cell Infect Microbiol* 2023;**13**:1291816.
14. Zhao S, Li Y, Fu S, Liu M, Li F, Liu C, et al. *Environmental factors and spatiotemporal distribution of Japanese encephalitis after vaccination campaign in Guizhou Province, China (2004-2016). BMC Infect Dis* 2021;**21**(1):1172.
15. Liu Z, Zhang Y, Tong MX, Zhang Y, Xiang J, Gao Q, et al. *Nonlinear and threshold effect of meteorological factors on Japanese Encephalitis Transmission in Southwestern China. Am J Trop Med Hyg* 2020;**103**(6):2442–9.
16. Wang LP, Yuan Y, Liu YL, Lu QB, Shi LS, Ren X, et al. *Etiological and epidemiological features of acute meningitis or encephalitis in China: a nationwide active surveillance study. Lancet Reg Health West Pac* 2022;**20**:100361.
17. Quan TM, Thao TTN, Duy NM, Nhat TM, Clapham H. *Estimates of the global burden of Japanese encephalitis and the impact of vaccination from 2000-2015. Elife* 2020;**9**:e51027.
18. Ni H, Cai X, Ren J, Dai T, Zhou J, Lin J, et al. *Epidemiological characteristics and transmission dynamics of dengue fever in China. Nat Commun* 2024;**15**(1):8060.
19. Zeng Q, Yu X, Ni H, Xiao L, Xu T, Wu H, et al. *Dengue transmission dynamics prediction by combining metapopulation networks and Kalman filter algorithm. PLoS Negl Trop Dis* 2023;**17**(6):e0011418.
20. He D, Ionides EL, King AA. *Plug-and-play inference for disease dynamics: measles in large and small populations as a case study. J R Soc Interface* 2010;**7**(43):271–83.
21. Shaman J, Karspeck A, Yang W, Tamerius J, Lipsitch M. *Real-time influenza forecasts during the 2012-2013 season. Nat Commun* 2013;**4**:2837.
22. Pei S, Kandula S, Yang W, Shaman J. *Forecasting the spatial transmission of influenza in the United States. Proc Natl Acad Sci USA* 2018;**115**(11):2752–7.
23. Chinese Center for Disease Control and Prevention. Guidelines for the prevention and control of infectious diseases (WS 214–2008); 2021. ⟨https://icdc.chinacdc.cn/zcfgybz/bz/202112/P020211202500622258522.pdf⟩.
24. Guo Y, Wu H, Liu X, Yue Y, Ren D, Zhao N, et al. *National vectors surveillance report on mosquitoes in China, 2018. Chin J Vector Biol Control* 2019;**30**(2):128–33.
25. Zhao N, Guo Y, Wu H, Liu X, Yue Y, Ren D, et al. *National vectors surveillance report on mosquitoes in China, 2019. Chin J Vector Biol Control* 2020;**31**(4):395–400.
26. Chen L, Xing Y, Zhang Y, Xie J, Su B, Jiang J, et al. *Long-term variations of urban-Rural disparities in infectious disease burden of over 8.44 million children, adolescents, and youth in China from 2013 to 2021: an observational study. PLoS Med* 2024;**21**(4):e1004374.
27. Xing W, Liao Q, Viboud C, Zhang J, Sun J, Wu JT, et al. *Hand, foot, and mouth disease in China, 2008-12: an epidemiological study. Lancet Infect Dis* 2014;**14**(4):308–18.
28. Yu H, Alonso WJ, Feng L, Tan Y, Shu Y, Yang W, et al. *Characterization of regional influenza seasonality patterns in China and implications for vaccination strategies: spatio-temporal modeling of surveillance data. PLoS Med* 2013;**10**(11):e1001552.
29. Naumova EN, Jagai JS, Matyas B, DeMaria A, Jr, MacNeill IB, et al. *Seasonality in six enterically transmitted diseases and ambient temperature. Epidemiol Infect* 2007;**135**(2):281–92.
30. Xia Q, Yang Y, Zhang Y, Zhou L, Ma X, Xiao C, et al. *Shift in dominant genotypes of Japanese encephalitis virus and its impact on current vaccination strategies. Front Microbiol* 2023;**14**:1302101.
31. Wei J, Wang X, Zhang J, Guo S, Pang L, Shi K, et al. *Partial cross-protection between Japanese encephalitis virus genotype I and III in mice. PLoS Negl Trop Dis* 2019;**13**(8):e0007601.
32. Tao Z, Liu G, Wang M, Wang H, Lin X, Song L, et al. *Molecular epidemiology of Japanese encephalitis virus in mosquitoes during an outbreak in China, 2013. Sci Rep* 2014;**4**:4908.
33. Zheng Y, Li M, Wang H, Liang G. *Japanese encephalitis and Japanese encephalitis virus in mainland China. Rev Med Virol* 2012;**22**(5):301–22.

34. Chen Y, Liu T, Yu X, Zeng Q, Cai Z, Wu H, et al. *An ensemble forecast system for tracking dynamics of dengue outbreaks and its validation in China. PLoS Comput Biol* 2022;**18**(6):e1010218.
35. Pei S, Yamana TK, Kandula S, Galanti M, Shaman J. *Burden and characteristics of COVID-19 in the United States during 2020. Nature* 2021;**598**(7880):338–41.
36. DeJohn A, Liu B, Ma X, Widener MJ, Liu Z. *Mobility, ICT, and health: a built environment investigation of older Chinese migrants' social isolation and loneliness. BMC Public Health* 2025;**25**(1):513.
37. Stein MV, Brooks SK, Smith LE, Rubin GJ, Amlôt R, Greenberg N, et al. *The impact of self-isolation due to COVID-19 on health care workers' mental health and wellbeing: a systematic review with narrative synthesis. medRxiv* 2025. https://doi.org/10.1101/2025.02.18.25322220 [Preprint].
38. Pei S, Cane MA, Shaman J. *Predictability in process-based ensemble forecast of influenza. PLoS Comput Biol* 2019;**15**(2):e1006783.
39. Pei S, Shaman J. *Counteracting structural errors in ensemble forecast of influenza outbreaks. Nat Commun* 2017;**8**(1):925.
40. Puspita JW, Fakhruddin M, Nuraini N, Soewono E. *Time-dependent force of infection and effective reproduction ratio in an age-structure dengue transmission model in Bandung City, Indonesia. Infect Dis Model* 2022;**7**(3):430–47.
41. Gao X, Li X, Li M, Fu S, Wang H, Lu Z, et al. *Vaccine strategies for the control and prevention of Japanese encephalitis in Mainland China, 1951-2011. PLoS Negl Trop Dis* 2014;**8**(8):e3015.
42. Mulvey P, Duong V, Boyer S, Burgess G, Williams DT, Dussart P, et al. *The ecology and evolution of Japanese encephalitis virus. Pathogens* 2021;**10**(12):1534.
43. van den Hurk AF, Ritchie SA, Mackenzie JS. *Ecology and geographical expansion of Japanese encephalitis virus. Annu Rev Entomol* 2009;**54**:17–35.
44. Diallo AOI, Chevalier V, Cappelle J, Duong V, Fontenille D, Duboz R. *How much does direct transmission between pigs contribute to Japanese Encephalitis virus circulation? A modelling approach in Cambodia. PLoS One* 2018;**13**(8):e0201209.
45. van den Driessche P. *Reproduction numbers of infectious disease models. Infect Dis Model* 2017;**2**(3):288–303.
46. Parag KV, Obolski U. *Risk averse reproduction numbers improve resurgence detection. PLoS Comput Biol* 2023;**19**(7):e1011332.
47. Jung SM, Endo A, Akhmetzhanov AR, Nishiura H. *Predicting the effective reproduction number of COVID-19: inference using human mobility, temperature, and risk awareness. Int J Infect Dis* 2021;**113**:47–54.
48. Li G, Li X, Chen J, Lemey P, Vrancken B, Su S, et al. *Tracing more than two decades of Japanese encephalitis virus circulation in mainland China. J Virol* 2025;**99**:e0157524.
49. Wang LY, Zhang WY, Ding F, Hu WB, Soares Magalhaes RJ, Sun HL, et al. *Spatiotemporal patterns of Japanese encephalitis in China, 2002-2010. PLoS Negl Trop Dis* 2013;**7**(6):e2285.
50. Wang LP, Yuan Y, Liu YL, Lu QB, Shi LS, Ren X, et al. *Etiological and epidemiological features of acute meningitis or encephalitis in China: a nationwide active surveillance study. Lancet Reg Health West Pac* 2022;**20**:100361.
51. Oidtman RJ, Lai S, Huang Z, Yang J, Siraj AS, Reiner RC, et al. *Inter-annual variation in seasonal dengue epidemics driven by multiple interacting factors in Guangzhou, China. Nat Commun* 2019;**10**(1):1148.
52. Gibb R, Colón-González FJ, Lan PT, Huong PT, Nam VS, Duoc VT, et al. *Interactions between climate change, urban infrastructure and mobility are driving dengue emergence in Vietnam. Nat Commun* 2023;**14**(1):8179.
53. Viboud C, Bjørnstad ON, Smith DL, Simonsen L, Miller MA, Grenfell BT. *Synchrony, waves, and spatial hierarchies in the spread of influenza. Science* 2006;**312**(5772):447–51.
54. Tizzoni M, Bajardi P, Poletto C, Ramasco JJ, Balcan D, Gonçalves B, et al. *Real-time numerical forecast of global epidemic spreading: case study of 2009 A/H1N1pdm. BMC Med* 2012;**10**:165.
55. Herstein JJ, Lowe JJ, Wolf T, Vasoo S, Leo YS, Chin BS, et al. *Leveraging a Preexisting Global Infectious Disease Network for local decision making during a pandemic. Clin Infect Dis* 2022;**74**(4):729–33.
56. Bjørnstad ON, Shea K, Krzywinski M, Altman N. *The SEIRS model for infectious disease dynamics. Nat Methods* 2020;**17**(6):557–8.
57. Kong JD, Davis W, Wang H. *Dynamics of a cholera transmission model with immunological threshold and natural phage control in reservoir. Bull Math Biol* 2014;**76**(8):2025–51.
58. Schuh AJ, Ward MJ, Leigh Brown AJ, Barrett AD. *Dynamics of the emergence and establishment of a newly dominant genotype of Japanese encephalitis virus throughout Asia. J Virol* 2014;**88**(8):4522–32.